Prefrontal Lesions Disrupt Posterior Alpha–Gamma Coordination of Visual Working Memory Representations

Saeideh Davoudi[1,2,3], Mohsen Parto Dezfouli[3,4], Robert T. Knight[5], Mohammad Reza Daliri[3,4], and Elizabeth L. Johnson[5,6]

Abstract

■ How does the human brain prioritize different visual representations in working memory (WM)? Here, we define the oscillatory mechanisms supporting selection of "where" and "when" features from visual WM storage and investigate the role of pFC in feature selection. Fourteen individuals with lateral pFC damage and 20 healthy controls performed a visuospatial WM task while EEG was recorded. On each trial, two shapes were presented sequentially in a top/bottom spatial orientation. A retro-cue presented mid-delay prompted which of the two shapes had been in either the top/bottom spatial position or first/second temporal position. We found that cross-frequency coupling between parieto-occipital alpha (α; 8–12 Hz) oscillations and topographically distributed gamma (γ; 30–50 Hz) activity tracked selection of the distinct cued feature in controls. This signature of feature selection was disrupted in patients with pFC lesions, despite intact α–γ coupling independent of feature selection. These findings reveal a pFC-dependent parieto-occipital α–γ mechanism for the rapid selection of visual WM representations. ■

INTRODUCTION

We are constantly bombarded with incoming information, necessitating focus on information relevant to current goals. Working memory (WM) provides the neurocognitive infrastructure to maintain and select information relevant to current goals (Miller, Lundqvist, & Bastos, 2018; Nyberg & Eriksson, 2016; Eriksson, Vogel, Lansner, Bergström, & Nyberg, 2015; Cowan, 2014). Selecting relevant information from WM stores is supported by attentional mechanisms that prioritize certain mnemonic representations while filtering out the rest (Poch, Capilla, Hinojosa, & Campo, 2017; Bledowski, Rahm, & Rowe, 2009; Oberauer & Bialkova, 2009; Awh, Vogel, & Oh, 2006; Courtney, 2004; Kastner & Pinsk, 2004; Curtis & D'Esposito, 2003; Oberauer, 2002; Awh & Jonides, 2001). Although it is understood that attention is involved in WM, how the human brain rapidly selects which information is relevant to rapidly changing goals remains a focus of debate.

Dr. Donald T. Stuss was pivotal in establishing the critical role of the pFC in attention. Based on decades of observations that discrete lesions to pFC diminish attentional performance and corresponding neural responses, Stuss et al. solidified the role of pFC in attention (Stuss & Knight, 2013; Stuss, 2006, 2011). Accordingly, pFC is posited to support WM through attentional mechanisms that select relevant information from mnemonic representations stored in posterior sensory regions (Parto Dezfouli, Zarei, Constantinidis, & Daliri, 2021; Sreenivasan, Curtis, & D'Esposito, 2014; Szczepanski & Knight, 2014). By comparing EEG in patients with unilateral pFC lesions to age- and education-matched controls, our group demonstrated that low-frequency (2–7 Hz) neural oscillations support pFC control over posterior visual regions during visual WM (Johnson et al., 2017). This finding is in accord with nonhuman primate studies showing direct projections from lateral frontal regions, including frontal eye fields, to visual cortex (Merrikhi, Clark, & Noudoost, 2018; Merrikhi et al., 2017), linking structure to function through neural oscillations in pFC.

However, according to the "gating by inhibition" hypothesis, oscillations in the alpha band (α; 8–12 Hz) support selective attention by inhibiting task-irrelevant information in posterior visual regions (Van Diepen, Foxe, & Mazaheri, 2019; Wianda & Ross, 2019; van Ede, 2018; Bengson, Mangun, & Mazaheri, 2012; Bonnefond & Jensen, 2012; Freunberger, Werkle-Bergner, Griesmayr, Lindenberger, & Klimesch, 2011; Jensen & Mazaheri, 2010; Jokisch & Jensen, 2007; Jensen, Gelfand, Kounios, & Lisman, 2002). Whereas α suppression induces neuronal excitability and activates visual inputs, phasic α enhancement deactivates task-irrelevant inputs (Jensen & Mazaheri, 2010). These

[1]University of Montréal, Quebec, Canada, [2]CHU Sainte-Justine Research Center, Montréal, Quebec, Canada, [3]Biomedical Engineering Department, School of Electrical Engineering, Iran University of Science and Technology (IUST), Tehran, Iran, [4]School of Cognitive Sciences (SCS), Institute for Research in Fundamental Sciences (IPM), Tehran, Iran, [5]University of California, Berkeley, [6]Wayne State University, Detroit, Michigan

Journal of Cognitive Neuroscience 33:9, pp. 1798–1810
https://doi.org/10.1162/jocn_a_01715

attention-related modulations of α activity are thought to support WM both by engaging cortical regions that may be necessary for task performance (e.g., visual regions during visual WM) and by filtering out task-irrelevant, distracting inputs (from visual WM representations; de Vries, Slagter, & Olivers, 2020; Jensen & Mazaheri, 2010; Sauseng et al., 2009). Indeed, modulations of α activity have been shown to guide attention to different features of stimuli in WM using visual (Schneider, Mertes, & Wascher, 2016) as well as auditory retro-cue tasks (Backer, Binns, & Alain, 2015; Lim, Wöstmann, & Obleser, 2015).

In the same EEG study where we demonstrated that low-frequency (2–7 Hz) neural oscillations support pFC control over posterior visual regions during visual WM (Johnson et al., 2017), we also demonstrated posterior α power suppression during the maintenance and processing of visual WM representations. These results link α suppression to recruitment of task-relevant visual regions, and, importantly, this α power suppression mechanism was independent of pFC damage. It is unknown whether posterior α mechanisms might similarly support "gating by inhibition" independent of pFC, or whether manipulating attention to different visual representations in WM might reveal a dissociable inhibitory α mechanism that depends on pFC.

Cross-frequency coupling, where the phase of α oscillations modulates the amplitude of activity in the gamma band (γ; 30–50 Hz), provides a putative mechanism for inhibition in WM (de Vries et al., 2020; Bonnefond & Jensen, 2015; Roux & Uhlhaas, 2014). We hypothesized that trial-by-trial shifts in the coupling of γ activity to parieto-occipital α oscillations (i.e., α–γ phase-amplitude coupling [PAC]) would index the selection of relevant features from visual WM stores. Phasic α enhancement in visual cortex would thus prioritize stimulus-specific γ representations by inhibiting task-irrelevant distractors (Jensen, Gips, Bergmann, & Bonnefond, 2014; Haegens, Nácher, Luna, Romo, & Jensen, 2011), supporting WM.

To test this hypothesis, we analyzed EEG data from a study conducted in a large cohort of patients with unilateral pFC lesions that required the selection of spatial and temporal features (i.e., top, bottom, first, second) from visual WM stores (Johnson et al., 2017). We chose to use this neurological data set given the documented observation of pFC-independent α power suppression during the maintenance and processing of visual WM representations, as described above. Here, we tested whether patterns of α–γ PAC would likewise index feature selection independent of pFC, or rather depend on pFC. To quantify feature selection, we compared selection of the top versus bottom spatial feature and first versus second temporal feature within the control group. To further delineate topographical patterns of α–γ PAC during feature selection, we applied graph theory. Systematic variation in patterns of α–γ PAC would indicate feature selection, supporting our hypothesis. We then investigated the role of pFC in an interaction approach by comparing feature selection between the control and pFC lesion groups.

METHODS

Participants

Participants were 14 patients with discrete pFC lesions (five men; mean ± *SD* [range]: 46 ± 16 [20–71] years of age, 15 ± 3 years of education) and 20 healthy controls (11 men; 44 ± 19 [19–70] years of age, 16 ± 3 years of education). Lesions were unilateral (n = 7 left + 7 right hemisphere) with maximal lesion overlap in dorsolateral pFC (Figure 1). All lesions were chronic (7.63 ± 5.98 [0.75–18] years elapsed) and due a single stroke (n = 5) or surgical resection of a low-grade tumor (n = 9). All participants had a normal/corrected-to-normal vision; all patients were evaluated by a neurologist and had no other neurological or psychiatric diagnoses. Patient IQ was normal or higher. For additional details about individual lesion etiology, see Johnson et al. (2017). All participants gave written informed consent in accordance with the Declaration of Helsinki.

Behavioral Task

Feature selection was examined in a single-trial visuospatial WM task paradigm that has been reported previously (Figure 2A; Parto Dezfouli, Davoudi, Knight, Daliri, & Johnson, 2021; Johnson et al., 2017, 2018, 2019). Following a 2-sec fixation, an 800-msec starting screen indicated that the upcoming stimuli would be tested on either spatiotemporal relations or stimulus identities. At encoding, two colored shapes were presented sequentially (200 msec each) in a top/bottom spatial orientation, separated by a 200-msec interstimulus interval. Shapes were presented to either the left or right visual hemifield. A retro-cue was presented mid-delay after a randomly jittered 900/1150-msec maintenance interval, followed by a postcue processing interval of the same length. On spatiotemporal relation trials, the retro-cue was one of four words—TOP, BOTTOM, FIRST, or SECOND—and participants subsequently responded by indicating which of two stimuli matched the cued position. These stimuli, presented on the subsequent response screen, were the same two shapes that had been presented at encoding, and WM was assessed in a two-alternative forced choice test. On identity control trials, the retro-cue SAME prompted participants to attend to the identities of both encoding stimuli, regardless of their spatiotemporal relationship. Participants completed 120–240 trials (80–160 spatiotemporal relation trials) of the task.

We tested feature selection by comparing the selection of TOP and BOTTOM spatial and FIRST and SECOND temporal features during the postcue processing interval. Because identity control trials did not require orienting attention to different features, we restricted analyses to spatiotemporal relation trials. Because the visual field of presentation was not relevant to the WM task and did not affect behavior (Johnson et al., 2017), to increase statistical power, we pooled the four spatiotemporal trial types across left and right presentations.

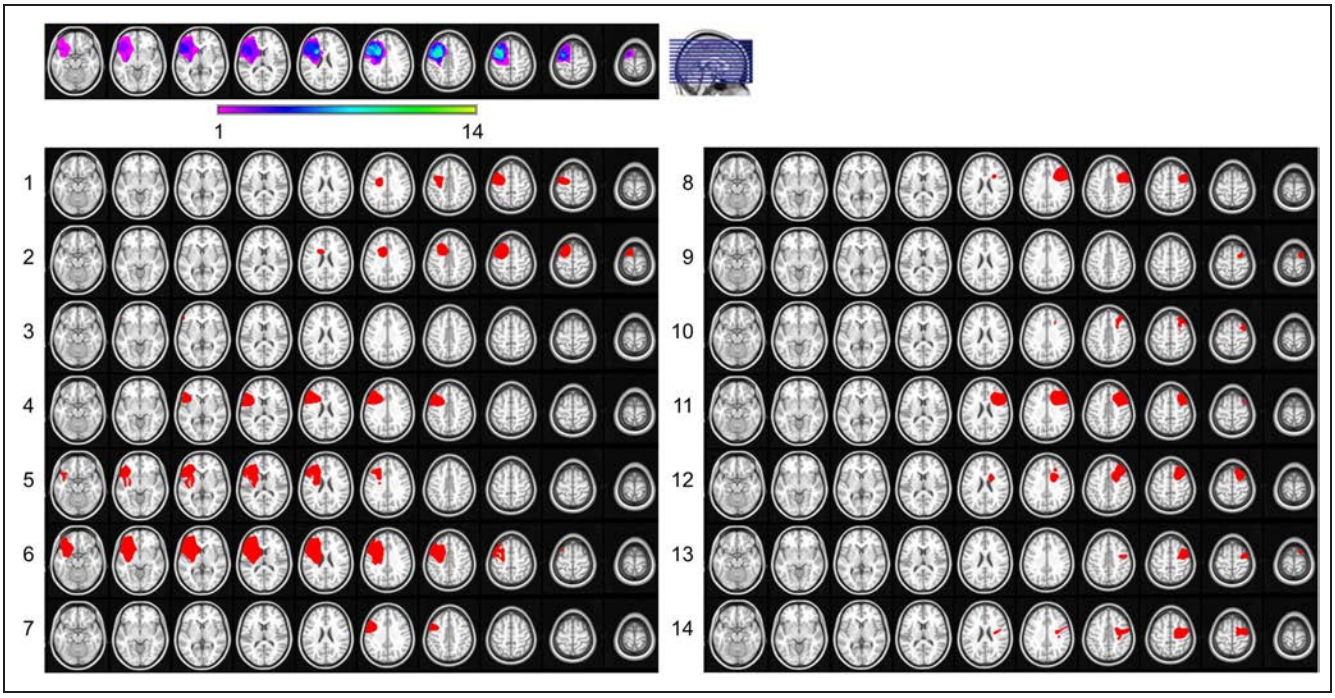

Figure 1. pFC lesions. Reconstruction of the extent of lesion overlap for all 14 patients, normalized to the left hemisphere, shows maximal overlap in dorsolateral pFC (top). Color scale, number of patients with lesions at the specified site. pFC lesions were in the left hemisphere of seven patients and right hemisphere of seven patients (bottom). Adapted from Johnson et al. (2017).

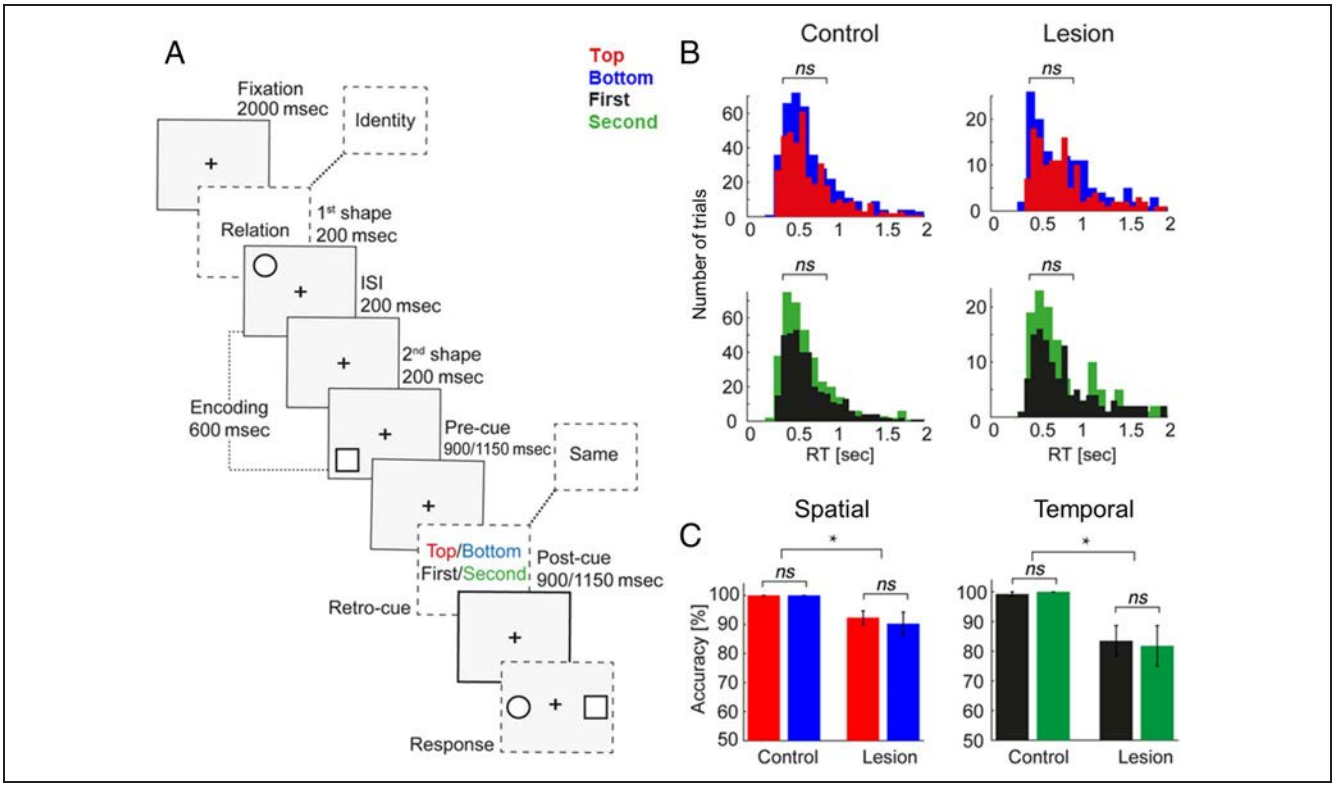

Figure 2. Visuospatial WM task and behavior. (A) WM task. At encoding, two shapes were presented sequentially (200 msec each, 200-msec interstimulus interval) in a top/bottom spatial orientation. After a randomly jittered 900/1150-msec maintenance interval, participants were cued to identify which shape had been presented in the TOP/BOTTOM spatial position or FIRST/SECOND temporal position during a postcue processing interval of the same length (spatiotemporal relation trials; analyzed here). In one third of trials, participants were cued to continue maintaining a representation of what the shapes looked like (identity control trials; not analyzed). WM was tested in a two-alternative forced choice test (50% chance). (B) RT did not differ between spatial or temporal features in either group. (C) Accuracy did not differ between spatial or temporal features in either group. Accuracy was attenuated in pFC patients relative to controls. *Significant; error bars, *SEM*.

To ensure that selection of different features was equally difficult (Poncet, Baudouin, Dzhelyova, Rossion, & Leleu, 2019), we compared behavioral response times (RTs; all correct trials with RT ≤ 2 sec) and accuracy (percent correct) between TOP and BOTTOM spatial and FIRST and SECOND temporal trials using Wilcoxon rank sum tests. pFC lesion effects were confirmed by comparing overall spatial (i.e., pooled TOP and BOTTOM trials) and temporal (FIRST and SECOND) accuracy between the control and patient groups using Wilcoxon rank sum tests. Because several pFC lesion patients had slowed motor responses following stroke, we did not compare RT between groups.

Data Acquisition and Preprocessing

EEG data were recorded using a 64+8 channel BioSemi ActiveTwo amplifier with Ag-AgCl pin-type active electrodes mounted on an elastic cap according to the International 10–20 System, sampled at 1024 Hz. Continuous eye gaze positions were recorded using an Eyelink 1000 (SR Research) or iView X optical tracker (SMI). A custom wooden chin rest was used to restrict participants' head movements to minimize contamination of the EEG signal in anterior channels.

Raw EEG data were referenced to the mean of both earlobes, down-sampled to 256 Hz, and filtered between 1 and 70 Hz using finite impulse response filters. Electromyography artifacts were removed automatically, and line noise was removed using discrete Fourier transform. Continuous data were segmented into trials, noisy channels were rejected, and independent components analysis was used to remove artifacts (e.g., electrooculogram artifacts, heartbeat, auricular components, and residual cranial muscle activity) from remaining channels (Hipp & Siegel, 2013). Any rejected channels were then reconstructed by interpolation of the mean of the nearest neighboring channels, and trials with residual noise were removed manually based on visual inspection. The final data set included an average of 101 ± 23 trials per participant. We randomly removed trials to equate the number of trials of each spatiotemporal feature per participant, resulting in an average of 23 ± 7 trials analyzed per feature.

The surface Laplacian spatial filter was applied to artifact-free data to minimize volume conduction and increase the robustness of signal source (Cohen, 2015; Perrin, Pernier, Bertrand, & Echallier, 1989). Then, channels were swapped across the midline in the data of right-hemisphere lesion patients (n = 7 of 14) to normalize lesions to the left hemisphere. This procedure removes individual differences between left- and right-hemisphere lesioned patients and increases statistical power in the lesion group. The same swapping procedure was applied to 10 of 20 randomly chosen control data sets so any interhemispheric variation was removed from both groups (Johnson et al., 2017).

Finally, previous analysis of this data set indicated that pFC lesions impacted pFC activity at baseline (Parto Dezfouli, Davoudi, et al., 2021; Johnson et al., 2017). To equate signal amplitude between individuals, we z-score-normalized every participant's spatial-filtered data in the time domain before analysis (Vaidya, Pujara, Petrides, Murray, & Fellows, 2019; Cole & Voytek, 2017; Gerber, Sadeh, Ward, Knight, & Deouell, 2016). We then analyzed the Laplacian-transformed, z-score-normalized EEG data over the 900-msec postcue processing interval of all correct spatiotemporal relation trials.

Power Spectral Density

We used a Hamming window based on a 900-msec periodogram to perform spectral decomposition at each frequency from 2 to 50 Hz. Power was computed per trial at all 64 Laplacian-transformed channels and then averaged across trials per participant. We then took the means in five canonical frequency bands: delta (δ; 2–4 Hz), theta (θ; 4–7 Hz), alpha (α; 8–12 Hz), beta (β; 13–30 Hz), and gamma (γ; 30–50 Hz). Feature selection was quantified per participant in each frequency band as the absolute values of TOP–BOTTOM and FIRST–SECOND trial differences.

Cross-Frequency Coupling

PAC was computed using the oscillation-triggered coupling (OTC) method (Dvorak & Fenton, 2014). This method employs a data-driven, event-based, and parameter-free algorithm to quantify PAC in four steps:

i) Spectral decomposition: Trials were padded by 4500 msec and pooled into a single time series, and the continuous wavelet transform was used to extract amplitude information at each frequency from 2 to 50 Hz. Time–frequency representations were obtained by convolving the Morlet wavelets (mw) with the EEG signal of a trial $x(t)$ as follows:

$$mw(t,f_0) = \left(\sigma_t\sqrt{\pi}\right)^{-1/2}\exp(2i\pi f_0 t) \qquad (1)$$

where t and f refer to time and frequency points, σ_t is the standard deviation in the time–domain, and $(\sigma_t\sqrt{\pi})^{-1/2}$ is a normalization factor to turn the wavelet energy to value 1.

ii) Trigger detection: Time–frequency representations were z-score normalized across all time points, and triggers were defined as $z > 2$ (i.e., $p < .05$) at each frequency. Triggers detected in the first or last 50 msec of each trial were considered noise from edges and excluded from analysis.

iii) OTC comodulogram: The EEG signal was fit within a window ± 200 msec around each trigger as follows:

$$\hat{x} = \sum_{n=1}^{N} x(n - TW \ldots n + TW) \qquad (2)$$

where n denotes the trigger time points, N denotes the number of trigger events, and TW denotes the time

window. The sum operator is used instead of the average to indicate the total number of trigger events. An OTC comodulogram is then generated from the mean across all triggers with time on the *x*-axis and amplitude frequencies on the *y*-axis. The frequency that shows an oscillatory pattern is the amplitude frequency coupled to the oscillatory pattern in the EEG signal, and the peak-to-peak amplitude indicates the modulation strength.

iv) PAC: The fast Fourier transform was applied to the OTC comodulogram to generate a PAC comodulogram with phase frequencies on the *x*-axis and amplitude frequencies on the *y*-axis. PAC was computed between all 64×64 Laplacian-transformed channel pairs in two sets of analyses (Ahmadi, Davoudi, & Daliri, 2019; Davoudi, Ahmadi, & Daliri, 2020; Johnson et al., 2018; Jones, Johnson, & Berryhill, 2020; van Wingerden, van der Meij, Kalenscher, Maris, & Pennartz, 2014).

First, we identified channel pairs exhibiting significant PAC across pooled spatial (TOP and BOTTOM) and temporal (FIRST and SECOND) trials. We used a permutation approach to define the channel pairs exhibiting PAC. For each channel-pair trigger event, we randomly shuffled the phase time series across time points (100 iterations) and recalculated PAC. This procedure breaks the temporal relationship between phase and amplitude time series without altering the amplitude time series or other aspects of the original data, thereby estimating PAC that would be expected solely by chance. If regularities exist in the data that are not related to the temporal relationship between phase and amplitude (e.g., individual differences the voltage of the amplitude signal or length of the time series), then they will be present in the permuted data. Significance was determined by comparing the observed PAC values against the permutation distributions (Aru et al., 2015; van Wijk, Jha, Penny, & Litvak, 2015; Dvorak & Fenton, 2014).

We used Wilcoxon rank sum tests with a false discovery rate (FDR) multiple-comparison correction of $q < 0.05$ to examine pFC effects, independent of feature selection, by comparing PAC between the control and pFC lesion groups. As an additional control, we compared PAC between groups during the continued maintenance of stimulus identities (i.e., pooled SAME trials). We did not observe significant pFC lesion effects on identity control trials and focus on PAC during spatiotemporal feature selection to test hypotheses.

Second, we computed PAC separately across each of the four spatiotemporal features (pooled TOP trials, pooled BOTTOM trials, etc.) to analyze feature selection. Feature selection was quantified per participant as the dB-corrected absolute values of TOP–BOTTOM and FIRST–SECOND trial differences as follows:

$$10 \times \log(|FFT_{C1} - FFT_{C2}|) \quad (3)$$

where $c1$ and $c2$ represent the OTC comodulograms generated at Step iii.

Graph Theory

We used graph theory to map the topographical distributions of phase and amplitude networks underlying PAC. According to graph theory, neural networks are collections of nodes (here, Laplacian-transformed channels) and internode connections or edges (PAC), summarized as adjacency matrices (Karwowski, Vasheghani Farahani, & Lighthall, 2019; Sporns, 2018). To define PAC adjacency matrices, we assessed the PAC data for network degrees (i.e., the weight of cross-frequency connections between each channel and all other channels) using a threshold of 70% relative to each participant's maximum (Jalili, 2017; Knyazev, Volf, & Belousova, 2015).

Statistical Analysis of Feature Selection

Statistical analyses of EEG data were performed using Wilcoxon rank sum tests with an FDR multiple-comparison correction of $q < 0.05$ (Benjamini & Hochberg, 1995). Feature selection was examined in controls and pFC lesion patients by comparing per-participant modulation values (i.e., TOP–BOTTOM and FIRST–SECOND absolute values) against zero. pFC effects were tested by comparing per-participant modulation values between the control and pFC lesion groups.

Linear mixed-effects models examined the specificity of pFC lesion effects on PAC modulation of feature selection. In all models, α–γ PAC modulation of feature selection was the dependent variable and participants were considered a random effect. Individual mean data were computed using the FDR-thresholded masks corresponding to PAC modulation differences between groups (see Figure 5B, 5D). To show that effects were not driven by pFC lesion effects on PAC independent of feature selection, group (control, lesion) and condition (no feature selection, feature selection) were modeled as fixed effects. To show that effects were not driven by pFC lesion effects on power modulation of feature selection at the phase or amplitude frequency, group was modeled as the fixed effect and α and γ power were modeled as random effects.

Data Availability

The data and custom-built MATLAB codes that support the current findings are deposited to the University of California, Berkeley, Collaborative Research in Computational Neuroscience (CRCNS) database (https://doi.org/10.6080/K0ZC811B), which is accessible with a free CRCNS account (crcns.org). Account registration requires compliance with the CRCNS Terms of Use and is approved by a central administrator independent of the data authors. Per the Terms of Use, data are made available only for scientific purposes, and any publications derived from the data must state that CRCNS is the source of the data and cite the original paper.

RESULTS

Behavior

We first compared per-participant mean behavioral RT and accuracy between features to ensure they were equal in difficulty. No significant differences were observed in RT between TOP and BOTTOM spatial (control p = .80, pFC lesion p = .40) or FIRST and SECOND temporal features (control p = .36, pFC lesion p = .86; Figure 2B). Likewise, no significant differences were observed in accuracy between spatial (control p = 1, pFC lesion p = .57) or temporal features (control p = .33, pFC lesion p = .59; Figure 2C). These null results ensure that variations in EEG patterns between features cannot be explained by differences in task difficulty in the control or lesion group.

We then confirmed the role of pFC in spatiotemporal WM by comparing per-participant mean accuracy (i.e., pooled TOP and BOTTOM trials, FIRST and SECOND trials) between the control and pFC lesion groups. Accuracy was impaired in the lesion group for both spatial (mean ± *SD* correct: control 99.5 ± 0.15% vs. pFC lesion 91.6 ± 0.36%, $p < 10^{-5}$) and temporal features (control 98.9 ± 0.35% vs. pFC lesion 83.7 ± 0.66%, $p < 10^{-5}$; Figure 2C). Because attention to the retro-cue on each trial was necessary to provide a correct response, above-chance accuracy in the lesion group (one-tailed t test, $p < 10^{-11}$) indicates that participants attended to the retro-cue. Indeed, retro-cues are consistently shown to promote WM by guiding attention and the observation of ceiling-level accuracy in controls is consistent with previous reports (Poncet et al., 2019; Viswanathan, Bharadwaj, & Shinn-Cunningham, 2019; Souza & Oberauer, 2016; Backer & Alain, 2012; Griffin & Nobre, 2003; Landman, Spekreijse, & Lamme, 2003).

Power Spectral Density

Power spectral analysis confirmed dominant oscillations in the α band prior to analysis of α–γ PAC. Peaks in the power spectra were observed in the α band in both the control and pFC lesion groups. Scalp distributions of peak power revealed α maximally in parieto-occipital channels (POz–Pz–PO8) in controls (Figure 3A). Although less robust, α peaks were present in the same parieto-occipital channels in pFC lesion patients (Figure 3B). These results demonstrate posterior α oscillations during the selection of spatiotemporal features from WM stores. Power in the γ band was distributed across the EEG topography in both the control and pFC lesion groups (Figure 3C, 3D).

We then compared the selection of different features in the α and γ frequency bands. No significant differences between spatial or temporal features were observed within the control or pFC lesion groups (all uncorrected ps > .1). Likewise, no significant differences were observed in spatial or temporal feature selection between groups (all uncorrected ps > .1). These null results suggest that any differences observed in α–γ PAC in the selection of different spatial or temporal features, or in feature selection between groups, cannot be attributed to α or γ power differences.

Cross-Frequency Coupling Signatures of Feature Selection

Analysis of PAC tested the hypothesis that parieto-occipital α oscillations coordinate stimulus-specific γ representations, tracking feature selection across spatiotemporal scales. We used a data-driven measure, OTC, to compute PAC between all channel pairs (Johnson et al., 2018; van

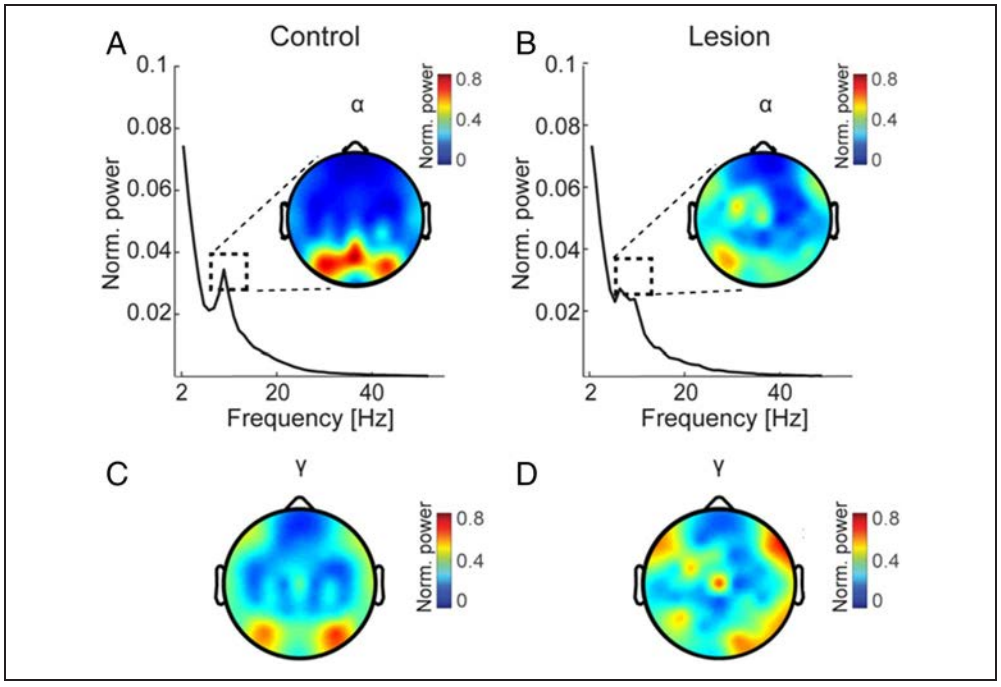

Figure 3. Posterior α oscillations and distributed γ activity during feature selection. (A–B) Mean α power across all trials during the postcue processing interval in controls (A) and pFC lesion patients (B). Dashed boxes indicate the peak frequency (8–12 Hz) corresponding to the scalp distributions. These α peaks were observed in both groups maximally at parieto-occipital channels (POz–Pz–PO8). (C–D) Mean γ (30–50 Hz) power across all trials during the postcue processing interval in controls (C) and pFC lesion patients (D). Scalp distributions indicate topographically distributed γ activity in both groups.

Wijk et al., 2015; FitzGerald, Valentin, Selway, & Richardson, 2013; Friese et al., 2013; Gregoriou, Gotts, Zhou, & Desimone, 2009). By treating increases in band-limited activity as discrete events, OTC provides an assumption-free measure of PAC that is appropriate for short time windows (Dvorak & Fenton, 2014). OTC outputs were analyzed using a permutation approach to account for differences in the input data and assess PAC significance (Aru et al., 2015; van Wijk et al., 2015; Dvorak & Fenton, 2014).

We first examined PAC during the selection of spatial and temporal features, independent of the specific feature (i.e., pooled TOP and BOTTOM trials, FIRST and SECOND trials). This analysis aimed to first determine the channel pairs exhibiting significant α–γ PAC and then test the role of pFC in α–γ PAC independent of feature selection. PAC was identified between posterior α oscillations and topographically distributed γ activity during the postcue processing interval in both groups ($p < .05$ compared to permuted PAC, uncorrected; Figure 4). pFC lesions did not significantly diminish α–γ PAC during the processing of spatial or temporal information (all uncorrected ps > .08). These null group effects reflect the results of statistical testing at each channel pair. Nonsignificant effects were replicated in independent tests of pooled spatial and pooled temporal trials, demonstrating that α–γ PAC was not markedly disrupted in patients with pFC lesions, independent of feature selection.

We next assessed whether α–γ PAC supported spatiotemporal feature selection in WM and whether prioritizing different visual representations might recruit pFC. In controls, spatial feature selection was identified in PAC between posterior α oscillations and topographically distributed γ activity (FDR-corrected $p < .05$; Figure 5A), thus linking feature selection to α–γ PAC. Although α–γ PAC also supported spatial feature selection in pFC lesion patients (FDR-corrected $p < .05$), α did not exhibit a posterior focus. pFC lesions diminished this PAC signature of spatial feature selection between α oscillations in parieto-occipital channels (P1–P3–PO3–POz–Pz) and γ activity in central-temporal channels (TP7–CP5–CP3–P5–P7–C5; FDR-corrected $p < .05$; Figure 5B, 5C). We identified comparable α–γ PAC patterns during temporal feature selection (FDR-corrected $p < .05$; Figure 5D). pFC lesions diminished temporal feature selection between α oscillations in the same parieto-occipital channels and γ activity in central-temporal channels (T7–TP7–P7–FC5–F7–F3; FDR-corrected $p < .05$; Figure 5E, 5F). Critically, channel pairs exhibiting significant modulation of spatial and

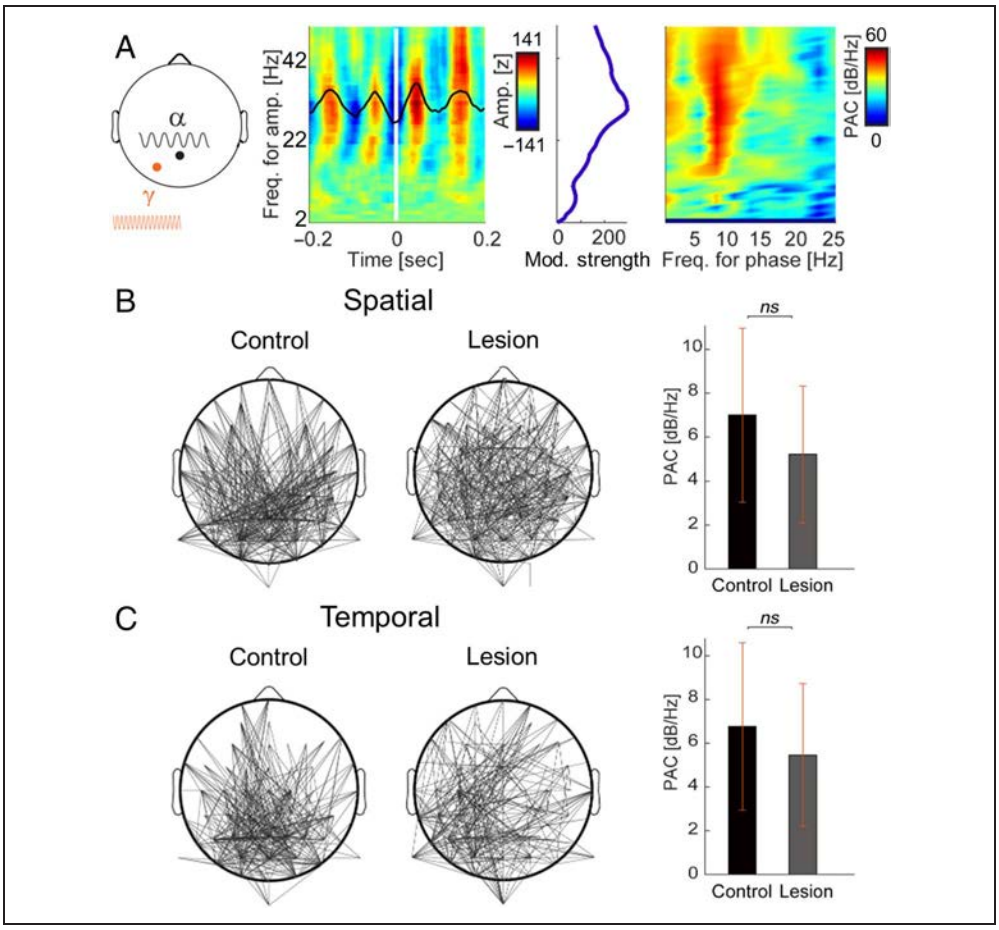

Figure 4. PAC does not depend on pFC independent of feature selection. (A) PAC in a representative posterior channel pair (Pz–PO3; left) during the processing of spatial features (i.e., pooled TOP and BOTTOM trials). Amplitude information was extracted per channel from 2 to 50 Hz, and OTC was quantified by averaging the EEG signal around increases in band-limited activity (i.e., triggers; middle). Modulation strength was maximal at γ amplitudes. PAC was computed by applying the fast Fourier transform to the OTC comodulogram (right). (B) Scalp distributions of α–γ PAC during the selection of spatial features in controls and pFC lesion patients, independent of the specific feature (i.e., pooled TOP and BOTTOM trials; left). Lines indicate channel pairs exhibiting significant PAC. Note PAC between posterior α oscillations and topographically distributed γ activity in both groups. Mean α–γ PAC across all significant pairs is shown for illustration (right). Error bars, *SEM*. (C) Same as (B) for temporal features (i.e., pooled FIRST and SECOND trials). Note similar scalp distributions of PAC in both groups.

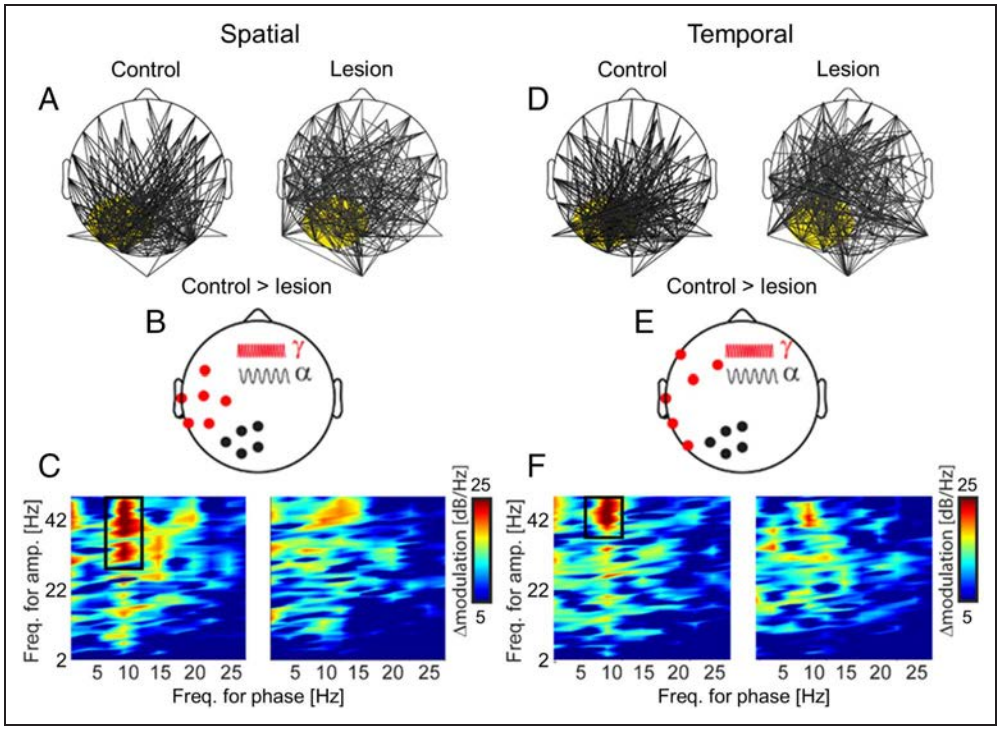

Figure 5. pFC lesions diminish PAC signatures of feature selection. (A) PAC between posterior α oscillations (focus marked in yellow) and topographically distributed γ activity modulated the selection of spatial features (i.e., TOP vs. BOTTOM) in controls and lesion patients. Lines indicate channel pairs of significant modulation. (B) pFC lesions diminished α–γ PAC modulation of spatial feature selection. Scalp distribution of α phase (black) and γ amplitude (red) channels contributing to significant modulation in controls > pFC lesion patients. (C) Mean PAC modulation of spatial feature selection across all channel pairs in (B) in controls (left) and pFC lesion patients (right). Note α–γ PAC modulation of spatial feature selection in controls (black box). PAC modulation was dimished with pFC lesions. (D–F) Same as (A–C) for the selection of temporal features (i.e., FIRST vs. SECOND). Note similar patterns and pFC lesion effects for spatial and temporal feature selection.

temporal features in controls exhibited diminished modulation with pFC lesions. These findings reveal that posterior α coordination of stimulus-specific γ representations supports feature selection, and this α–γ PAC signature depends on pFC.

Linear mixed-effects models confirmed the specificity of pFC lesion effects on α–γ PAC modulation of feature selection. Significant interactions between group and feature selection demonstrate that group differences in PAC modulation of feature selection were not driven by group differences in overall PAC (spatial: $F(1, 62) = 35.02, p = 2 \times 10^{-7}$; temporal: $F(1, 62) = 31.27, p = 6 \times 10^{-7}$; Figure 6). Likewise, group differences in PAC modulation of feature selection remained significant with power modulation of feature selection at the phase and amplitude frequencies modeled as random effects (spatial: $F(1, 31) = 36.79, p = 1 \times 10^{-6}$; temporal: $F(1, 31) = 18.04, p = 2 \times 10^{-4}$).

Last, we used graph theory to demonstrate that α oscillations coordinating feature selection were focused in parieto-occipital channels in controls but not pFC lesion patients. Analysis of the top 30% of cross-frequency connections (Jalili, 2017; Knyazev et al., 2015) indicated that PAC between parieto-occipital α oscillations and topographically distributed γ activity tracked the selection of spatial and temporal features in controls (Figure 7). Whereas γ channels supporting feature selection were widely distributed in both groups, α coordination of spatial and temporal features was not localized to parieto-occipital channels in

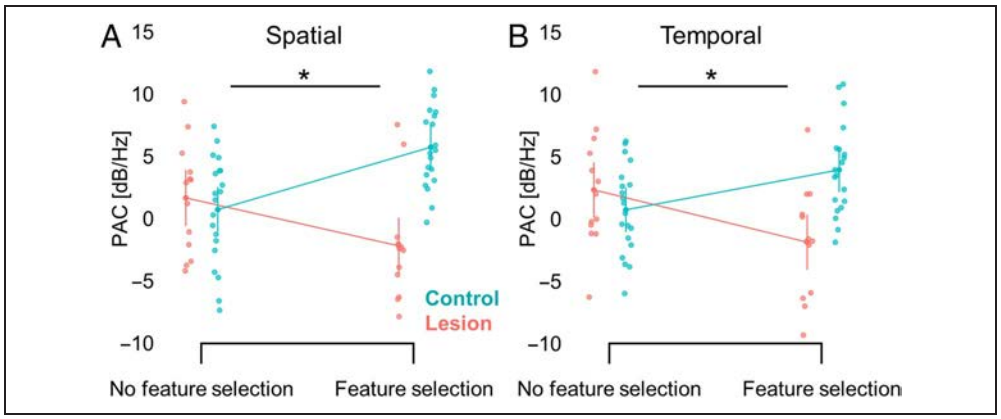

Figure 6. pFC lesions specifically affect PAC modulation of feature selection. (A) pFC lesions diminish PAC modulation of spatial feature selection (i.e., TOP vs. BOTTOM), and these results are not driven by an overall difference in PAC between groups (i.e., pooled TOP and BOTTOM trials). Error bars, *SEM*. (B) Same as (A) for temporal feature selection (i.e., FIRST vs. SECOND, pooled FIRST and SECOND trials).

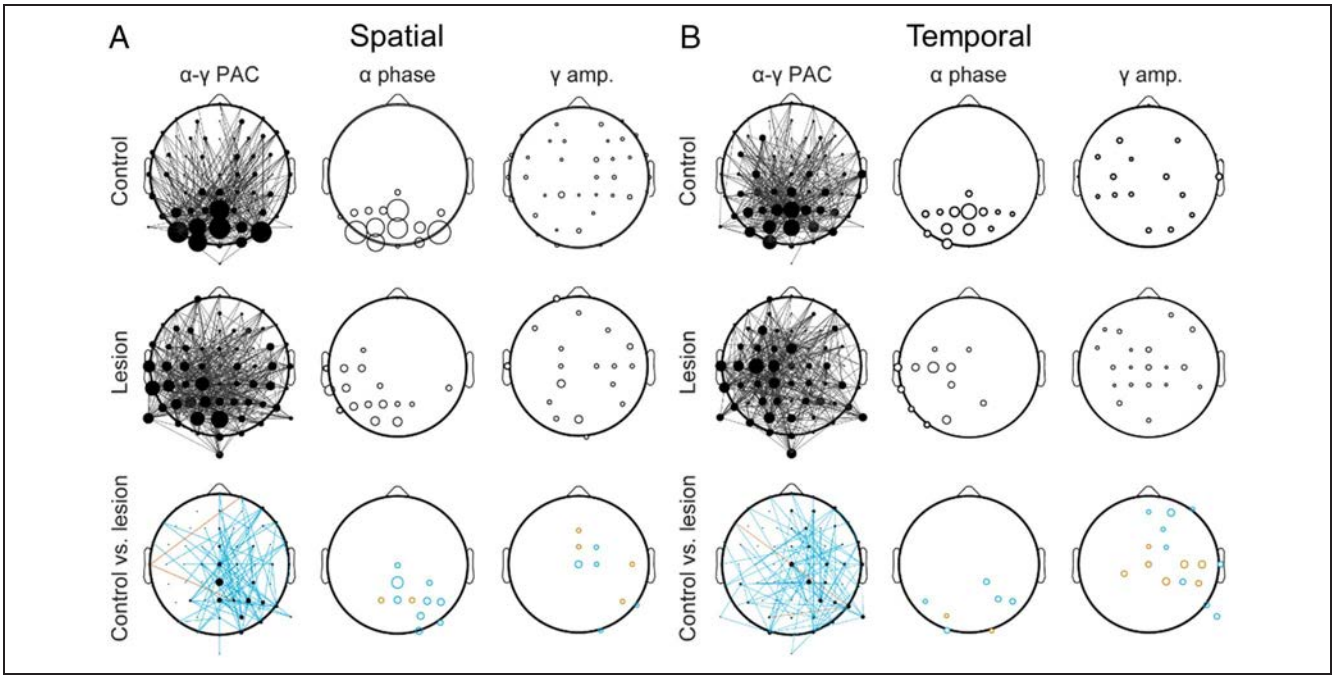

Figure 7. pFC lesions disrupt posterior α coordination of feature selection. (A) Scalp distributions of the top 30% of α–γ connections during spatial feature selection (i.e., TOP vs. BOTTOM) in controls (top), lesion patients (middle), and controls versus lesion patients (bottom). Lines indicate channel pairs exhibiting PAC (left), and the size of each circle indicates the relative number of cross-frequency connections at each α phase (middle) and γ amplitude (right) channel. Note the parieto-occipital focus of α channels in controls but not lesion patients. Turquoise, significant control > lesion; red, control < lesion. (B) Same as (A) for temporal feature selection (i.e., FIRST vs. SECOND).

pFC lesion patients. Between-groups testing confirmed that posterior α coordination of distributed γ activity was greater in controls than lesion patients (FDR-corrected $p < .05$). Thus, pFC lesions affect α–γ PAC signatures of feature selection by disrupting parieto-occipital α coordination of visual WM representations.

DISCUSSION

We demonstrate that parieto-occipital α coordination of visual WM representations depends on pFC. Specifically, cross-frequency coupling between parieto-occipital α oscillations and topographically distributed γ activity tracked the selection of spatiotemporal features from visual WM stores in controls. Patterns were similar during the selection of spatial and temporal features, suggesting a domain-general α–γ PAC signature of feature selection. These findings support the "gating by inhibition" hypothesis, which states that phasic α enhancement, indexed here by α–γ PAC, inhibits task-irrelevant information in visual regions (Van Diepen et al., 2019; Wianda & Ross, 2019; van Ede, 2018; Bengson et al., 2012; Bonnefond & Jensen, 2012; Freunberger et al., 2011; Jensen & Mazaheri, 2010; Jokisch & Jensen, 2007; Jensen et al., 2002). We show for the first time that this α–γ PAC signature of feature selection is disrupted with pFC lesions, revealing a pFC-dependent posterior α mechanism. In contrast, α–γ PAC was not significantly affected by pFC lesions independent of feature selection. Together, these findings suggest that α–γ PAC uniquely depends on pFC if the task demands inhibition of irrelevant representations in visual WM stores.

Previous analysis of this neurological data set revealed parieto-occipital α suppression during the maintenance and processing of visual WM representations in both controls and pFC lesion patients (Johnson et al., 2017). This result linked α suppression to the recruitment of task-relevant visual regions (Palva & Palva, 2011; Jensen & Mazaheri, 2010; Sauseng et al., 2009; Leiberg, Lutzenberger, & Kaiser, 2006), independent of pFC. In contrast, phasic α enhancement deactivates task-irrelevant visual inputs and filters out distracting information from visual WM representations (de Vries et al., 2020; Wianda & Ross, 2019; Freunberger et al., 2011; Jensen & Mazaheri, 2010; Sauseng et al., 2009; Jokisch & Jensen, 2007). Cross-frequency coupling between visual α oscillations and stimulus-specific γ representations is the purported mechanism for inhibition in visual WM (de Vries et al., 2020; Bonnefond & Jensen, 2015; Roux & Uhlhaas, 2014). This inhibitory α–γ mechanism is presumed to provide top–down control within the visual system (Bonnefond & Jensen, 2015; Jensen et al., 2014). Intriguingly, the current findings suggest that this inhibitory α–γ mechanism is only focused in visual regions in the intact brain. Whereas α oscillations contributing to feature selection were focused in parieto-occipital channels in controls, these α oscillations were distributed across central-temporal channels in pFC lesion patients. These findings evidence pFC-dependent parieto-occipital α coordination of stimulus-specific γ representations in the service of WM.

Interactions between pFC and posterior sensory regions are well-documented in studies of WM (Merrikhi et al., 2017, 2018; Mendoza-Halliday, Torres, & Martinez-Trujillo, 2014; Qi, Elworthy, Lambert, & Constantinidis, 2014; Hussar & Pasternak, 2013; Zaksas & Pasternak, 2006; Constantinidis, Franowicz, & Goldman-Rakic, 2001). Structurally, such interactions are supported by direct projections from lateral frontal regions, including frontal eye fields, to visual cortex (Merrikhi et al., 2017, 2018). Neural oscillations provide a plausible mechanism of such cortico–cortical interaction. Indeed, previous analysis of this neurological data set revealed a low-frequency (2–7 Hz) oscillatory mechanism supporting pFC control over parieto-occipital regions during WM, consistent with models of pFC control over visual mnemonic representations (Sreenivasan et al., 2014; Szczepanski & Knight, 2014). Further evidence for a direct relationship between low-frequency oscillations in pFC and α oscillations in parieto-occipital regions comes from a study of attention-guided visual perception (Helfrich, Huang, Wilson, & Knight, 2017). Taken together, these findings suggest that pFC exerts control over parieto-occipital α oscillations via low-frequency neural oscillations, aiding in the inhibition of task-irrelevant visual representations during WM.

Acknowledgments

We thank D. Scabini and A.-K. Solbakk for coordinating all patient testing efforts; C. D. Dewar, A.-K. Solbakk, T. Endestad, T. R. Meling, and J. Lubell for assistance testing patients; and C. D. Dewar for assistance with lesion and EEG data analysis.

Reprint requests should be sent to Elizabeth L. Johnson, Helen Wills Neuroscience Institute, University of California Berkeley, Knight Laboratory, Berkeley, CA, 94720-3190, or via e-mail: eljohnson@berkeley.edu; or Mohsen Parto Dezfouli, School of Cognitive Sciences (SCS), Institute for Research in Fundamental Sciences (IPM), Tehran, Iran, or via e-mail: moh3nparto@ipm.ir; or Mohammad Reza Daliri, Biomedical Engineering Department, School of Electrical Engineering, Iran University of Science and Technology, Tehran, Iran, or via e-mail: daliri@iust.ac.ir.

Author Contributions

Saeideh Davoudi: Conceptualization; Formal analysis; Methodology; Software; Validation; Visualization; Writing—Original draft. Mohsen Parto Dezfouli: Conceptualization; Formal analysis; Methodology; Software; Validation; Visualization; Writing—Original draft. Robert T. Knight: Funding acquisition; Project administration; Supervision; Writing—Review & editing. Mohammad Reza Daliri: Conceptualization; Supervision; Writing—Review & editing. Elizabeth L. Johnson: Conceptualization; Data curation; Formal analysis; Investigation; Methodology; Supervision; Visualization; Writing—Review & editing.

Funding Information

This work was supported by the National Institute of Neurological Disorders and Stroke (2R37NS21135, K99NS115918), James S. McDonnell Foundation (220020448), Research Council of Norway (240389/F20), and University of Oslo Internal Fund.

Diversity in Citation Practices

A retrospective analysis of the citations in every article published in this journal from 2010 to 2020 has revealed a persistent pattern of gender imbalance: Although the proportions of authorship teams (categorized by estimated gender identification of first author/last author) publishing in the *Journal of Cognitive Neuroscience (JoCN)* during this period were M(an)/M = .408, W(oman)/M = .335, M/W = .108, and W/W = .149, the comparable proportions for the articles that these authorship teams cited were M/M = .579, W/M = .243, M/W = .102, and W/W = .076 (Fulvio et al., *JoCN*, 33:1, pp. 3–7). Consequently, *JoCN* encourages all authors to consider gender balance explicitly when selecting which articles to cite and gives them the opportunity to report their article's gender citation balance.

REFERENCES

Ahmadi, A., Davoudi, S., & Daliri, M. R. (2019). Computer aided diagnosis system for multiple sclerosis disease based on phase to amplitude coupling in covert visual attention. *Computer Methods and Programs in Biomedicine*, *169*, 9–18. **DOI:** https://doi.org/10.1016/j.cmpb.2018.11.006, **PMID:** 30638593

Aru, J., Aru, J., Priesemann, V., Wibral, M., Lana, L., Pipa, G., et al. (2015). Untangling cross-frequency coupling in neuroscience. *Current Opinion in Neurobiology*, *31*, 51–61. **DOI:** https://doi.org/10.1016/j.conb.2014.08.002, **PMID:** 25212583

Awh, E., & Jonides, J. (2001). Overlapping mechanisms of attention and spatial working memory. *Trends in Cognitive Sciences*, *5*, 119–126. **DOI:** https://doi.org/10.1016/S1364-6613(00)01593-X, **PMID:** 11239812

Awh, E., Vogel, E. K., & Oh, S.-H. (2006). Interactions between attention and working memory. *Neuroscience*, *139*, 201–208. **DOI:** https://doi.org/10.1016/j.neuroscience.2005.08.023, **PMID:** 16324792

Backer, K. C., & Alain, C. (2012). Orienting attention to sound object representations attenuates change deafness. *Journal of Experimental Psychology: Human Perception and Performance*, *38*, 1554–1566. **DOI:** https://doi.org/10.1037/a0027858

Backer, K. C., Binns, M. A., & Alain, C. (2015). Neural dynamics underlying attentional orienting to auditory representations in short-term memory. *Journal of Neuroscience*, *35*, 1307–1318. **DOI:** https://doi.org/10.1523/JNEUROSCI.1487-14.2015, **PMID:** 25609643, **PMCID:** PMC6605545

Bengson, J. J., Mangun, G. R., & Mazaheri, A. (2012). The neural markers of an imminent failure of response inhibition. *Neuroimage*, *59*, 1534–1539. **DOI:** https://doi.org/10.1016/j.neuroimage.2011.08.034, **PMID:** 21889992

Benjamini, Y., & Hochberg, Y. (1995). Controlling the false discovery rate: A practical and powerful approach to multiple testing. *Journal of the Royal Statistical Society: Series B (Methodological)*, *57*, 289–300. **DOI:** https://doi.org/10.1111/j.2517-6161.1995.tb02031.x

Bledowski, C., Rahm, B., & Rowe, J. B. (2009). What "works" in working memory? Separate systems for selection and updating of critical information. *Journal of Neuroscience*, *29*,

13735–13741. **DOI:** https://doi.org/10.1523/JNEUROSCI.2547-09.2009, **PMID:** 19864586, **PMCID:** PMC2785708
Bonnefond, M., & Jensen, O. (2012). Alpha oscillations serve to protect working memory maintenance against anticipated distracters. *Current Biology*, *22*, 1969–1974. **DOI:** https://doi.org/10.1016/j.cub.2012.08.029, **PMID:** 23041197
Bonnefond, M., & Jensen, O. (2015). Gamma activity coupled to alpha phase as a mechanism for top–down controlled gating. *PLoS One*, *10*, e0128667. **DOI:** https://doi.org/10.1371/journal.pone.0128667, **PMID:** 26039691, **PMCID:** PMC4454652
Cohen, M. X. (2015). Comparison of different spatial transformations applied to EEG data: A case study of error processing. *International Journal of Psychophysiology*, *97*, 245–257. **DOI:** https://doi.org/10.1016/j.ijpsycho.2014.09.013, **PMID:** 25455427
Cole, S. R., & Voytek, B. (2017). Brain oscillations and the importance of waveform shape. *Trends in Cognitive Sciences*, *21*, 137–149. **DOI:** https://doi.org/10.1016/j.tics.2016.12.008, **PMID:** 28063662
Constantinidis, C., Franowicz, M. N., & Goldman-Rakic, P. S. (2001). The sensory nature of mnemonic representation in the primate prefrontal cortex. *Nature Neuroscience*, *4*, 311–316. **DOI:** https://doi.org/10.1038/85179, **PMID:** 11224549
Courtney, S. M. (2004). Attention and cognitive control as emergent properties of information representation in working memory. *Cognitive, Affective, & Behavioral Neuroscience*, *4*, 501–516. **DOI:** https://doi.org/10.3758/CABN.4.4.501, **PMID:** 15849893
Cowan, N. (2014). Working memory underpins cognitive development, learning, and education. *Educational Psychology Review*, *26*, 197–223. **DOI:** https://doi.org/10.1007/s10648-013-9246-y, **PMID:** 25346585, **PMCID:** PMC4207727
Curtis, C. E., & D'Esposito, M. (2003). Persistent activity in the prefrontal cortex during working memory. *Trends in Cognitive Sciences*, *7*, 415–423. **DOI:** https://doi.org/10.1016/S1364-6613(03)00197-9, **PMID:** 12963473
Davoudi, S., Ahmadi, A., & Daliri, M. R. (2020). Frequency–amplitude coupling: A new approach for decoding of attended features in covert visual attention task. *Neural Computing and Applications*, *33*, 3487–3502. **DOI:** https://doi.org/10.1007/s00521-020-05222-w
de Vries, I. E., Slagter, H. A., & Olivers, C. N. (2020). Oscillatory control over representational states in working memory. *Trends in Cognitive Sciences*, *24*, 150–162. **DOI:** https://doi.org/10.1016/j.tics.2019.11.006, **PMID:** 31791896
Dvorak, D., & Fenton, A. A. (2014). Toward a proper estimation of phase–amplitude coupling in neural oscillations. *Journal of Neuroscience methods*, *225*, 42–56. **DOI:** https://doi.org/10.1016/j.jneumeth.2014.01.002, **PMID:** 24447842, **PMCID:** PMC3955271
Eriksson, J., Vogel, E. K., Lansner, A., Bergström, F., & Nyberg, L. (2015). Neurocognitive architecture of working memory. *Neuron*, *88*, 33–46. **DOI:** https://doi.org/10.1016/j.neuron.2015.09.020, **PMID:** 26447571, **PMCID:** PMC4605545
FitzGerald, T. H., Valentin, A., Selway, R., & Richardson, M. P. (2013). Cross-frequency coupling within and between the human thalamus and neocortex. *Frontiers in Human Neuroscience*, *7*, 84. **DOI:** https://doi.org/10.3389/fnhum.2013.00084, **PMID:** 23532592, **PMCID:** PMC3607084
Freunberger, R., Werkle-Bergner, M., Griesmayr, B., Lindenberger, U., & Klimesch, W. (2011). Brain oscillatory correlates of working memory constraints. *Brain Research*, *1375*, 93–102. **DOI:** https://doi.org/10.1016/j.brainres.2010.12.048, **PMID:** 21172316
Friese, U., Köster, M., Hassler, U., Martens, U., Trujillo-Barreto, N., & Gruber, T. (2013). Successful memory encoding is associated with increased cross-frequency coupling between frontal theta and posterior gamma oscillations in human scalp-recorded EEG. *Neuroimage*, *66*, 642–647. **DOI:** https://doi.org/10.1016/j.neuroimage.2012.11.002, **PMID:** 23142278
Gerber, E. M., Sadeh, B., Ward, A., Knight, R. T., & Deouell, L. Y. (2016). Non-sinusoidal activity can produce cross-frequency coupling in cortical signals in the absence of functional interaction between neural sources. *PLoS One*, *11*, e0167351. **DOI:** https://doi.org/10.1371/journal.pone.0167351, **PMID:** 27941990, **PMCID:** PMC5152905
Gregoriou, G. G., Gotts, S. J., Zhou, H., & Desimone, R. (2009). Long-range neural coupling through synchronization with attention. *Progress in Brain Research*, *176*, 35–45. **DOI:** https://doi.org/10.1016/S0079-6123(09)17603-3
Griffin, I. C., & Nobre, A. C. (2003). Orienting attention to locations in internal representations. *Journal of Cognitive Neuroscience*, *15*, 1176–1194. **DOI:** https://doi.org/10.1162/089892903322598139, **PMID:** 14709235
Haegens, S., Nácher, V., Luna, R., Romo, R., & Jensen, O. (2011). α-Oscillations in the monkey sensorimotor network influence discrimination performance by rhythmical inhibition of neuronal spiking. *Proceedings of the National Academy of Sciences, U.S.A.*, *108*, 19377–19382. **DOI:** https://doi.org/10.1073/pnas.1117190108, **PMID:** 22084106, **PMCID:** PMC3228466
Helfrich, R. F., Huang, M., Wilson, G., & Knight, R. T. (2017). Prefrontal cortex modulates posterior alpha oscillations during top–down guided visual perception. *Proceedings of the National Academy of Sciences, U.S.A.*, *114*, 9457–9462. **DOI:** https://doi.org/10.1073/pnas.1705965114, **PMID:** 28808023, **PMCID:** PMC5584435
Hipp, J. F., & Siegel, M. (2013). Dissociating neuronal gamma-band activity from cranial and ocular muscle activity in EEG. *Frontiers in Human Neuroscience*, *7*, 338. **DOI:** https://doi.org/10.3389/fnhum.2013.00338, **PMID:** 23847508, **PMCID:** PMC3706727
Hussar, C. R., & Pasternak, T. (2013). Common rules guide comparisons of speed and direction of motion in the dorsolateral prefrontal cortex. *Journal of Neuroscience*, *33*, 972–986. **DOI:** https://doi.org/10.1523/JNEUROSCI.4075-12.2013, **PMID:** 23325236, **PMCID:** PMC3711598
Jalili, M. (2017). Graph theoretical analysis of Alzheimer's disease: Discrimination of AD patients from healthy subjects. *Information Sciences*, *384*, 145–156. **DOI:** https://doi.org/10.1016/j.ins.2016.08.047
Jensen, O., Gelfand, J., Kounios, J., & Lisman, J. E. (2002). Oscillations in the alpha band (9–12 Hz) increase with memory load during retention in a short-term memory task. *Cerebral Cortex*, *12*, 877–882. **DOI:** https://doi.org/10.1093/cercor/12.8.877, **PMID:** 12122036
Jensen, O., Gips, B., Bergmann, T. O., & Bonnefond, M. (2014). Temporal coding organized by coupled alpha and gamma oscillations prioritize visual processing. *Trends in Neurosciences*, *37*, 357–369. **DOI:** https://doi.org/10.1016/j.tins.2014.04.001, **PMID:** 24836381
Jensen, O., & Mazaheri, A. (2010). Shaping functional architecture by oscillatory alpha activity: Gating by inhibition. *Frontiers in Human Neuroscience*, *4*, 186. **DOI:** https://doi.org/10.3389/fnhum.2010.00186, **PMID:** 21119777, **PMCID:** PMC2990626
Johnson, E. L., Adams, J. N., Solbakk, A.-K., Endestad, T., Larsson, P. G., Ivanovic, J., et al. (2018). Dynamic frontotemporal systems process space and time in working memory. *PLoS Biology*, *16*, e2004274. **DOI:** https://doi.org/10.1371/journal.pbio.2004274, **PMID:** 29601574, **PMCID:** PMC5895055
Johnson, E. L., Dewar, C. D., Solbakk, A.-K., Endestad, T., Meling, T. R., & Knight, R. T. (2017). Bidirectional frontoparietal

oscillatory systems support working memory. *Current Biology*, *27*, 1829–1835. **DOI:** https://doi.org/10.1016/j.cub.2017.05.046, **PMID:** 28602658, **PMCID:** PMC5546232

Johnson, E. L., King-Stephens, D., Weber, P. B., Laxer, K. D., Lin, J. J., & Knight, R. T. (2019). Spectral imprints of working memory for everyday associations in the frontoparietal network. *Frontiers in Systems Neuroscience*, *12*, 65. **DOI:** https://doi.org/10.3389/fnsys.2018.00065, **PMID:** 30670953, **PMCID:** PMC6333050

Jokisch, D., & Jensen, O. (2007). Modulation of gamma and alpha activity during a working memory task engaging the dorsal or ventral stream. *Journal of Neuroscience*, *27*, 3244–3251. **DOI:** https://doi.org/10.1523/JNEUROSCI.5399-06.2007, **PMID:** 17376984, **PMCID:** PMC6672464

Jones, K. T., Johnson, E. L., & Berryhill, M. E. (2020). Frontoparietal theta-gamma interactions track working memory enhancement with training and tDCS. *Neuroimage*, *211*, 116615. **DOI:** https://doi.org/10.1016/j.neuroimage.2020.116615, **PMID:** 32044440, **PMCID:** PMC7733399

Karwowski, W., Vasheghani Farahani, F., & Lighthall, N. (2019). Application of graph theory for identifying connectivity patterns in human brain networks: A systematic review. *Frontiers in Neuroscience*, *13*, 585. **DOI:** https://doi.org/10.3389/fnins.2019.00585, **PMID:** 31249501, **PMCID:** PMC6582769

Kastner, S., & Pinsk, M. A. (2004). Visual attention as a multilevel selection process. *Cognitive, Affective, & Behavioral Neuroscience*, *4*, 483–500. **DOI:** https://doi.org/10.3758/CABN.4.4.483, **PMID:** 15849892

Knyazev, G. G., Volf, N. V., & Belousova, L. V. (2015). Age-related differences in electroencephalogram connectivity and network topology. *Neurobiology of Aging*, *36*, 1849–1859. **DOI:** https://doi.org/10.1016/j.neurobiolaging.2015.02.007, **PMID:** 25766772

Landman, R., Spekreijse, H., & Lamme, V. A. (2003). Large capacity storage of integrated objects before change blindness. *Vision Research*, *43*, 149–164. **DOI:** https://doi.org/10.1016/S0042-6989(02)00402-9, **PMID:** 12536137

Leiberg, S., Lutzenberger, W., & Kaiser, J. (2006). Effects of memory load on cortical oscillatory activity during auditory pattern working memory. *Brain Research*, *1120*, 131–140. **DOI:** https://doi.org/10.1016/j.brainres.2006.08.066, **PMID:** 16989782

Lim, S.-J., Wöstmann, M., & Obleser, J. (2015). Selective attention to auditory memory neurally enhances perceptual precision. *Journal of Neuroscience*, *35*, 16094–16104. **DOI:** https://doi.org/10.1523/JNEUROSCI.2674-15.2015, **PMID:** 26658862, **PMCID:** PMC6605502

Mendoza-Halliday, D., Torres, S., & Martinez-Trujillo, J. C. (2014). Sharp emergence of feature-selective sustained activity along the dorsal visual pathway. *Nature Neuroscience*, *17*, 1255–1262. **DOI:** https://doi.org/10.1038/nn.3785, **PMID:** 25108910, **PMCID:** PMC4978542

Merrikhi, Y., Clark, K., Albarran, E., Parsa, M., Zirnsak, M., Moore, T., et al. (2017). Spatial working memory alters the efficacy of input to visual cortex. *Nature Communications*, *8*, 15041. **DOI:** https://doi.org/10.1038/ncomms15041, **PMID:** 28447609, **PMCID:** PMC5414175

Merrikhi, Y., Clark, K., & Noudoost, B. (2018). Concurrent influence of top–down and bottom-up inputs on correlated activity of Macaque extrastriate neurons. *Nature Communications*, *9*, 5393. **DOI:** https://doi.org/10.1038/s41467-018-07816-4, **PMID:** 30568166, **PMCID:** PMC6300596

Miller, E. K., Lundqvist, M., & Bastos, A. M. (2018). Working memory 2.0. *Neuron*, *100*, 463–475. **DOI:** https://doi.org/10.1016/j.neuron.2018.09.023, **PMID:** 30359609

Nyberg, L., & Eriksson, J. (2016). Working memory: Maintenance, updating, and the realization of intentions. *Cold Spring Harbor Perspectives in Biology*, *8*, a021816. **DOI:** https://doi.org/10.1101/cshperspect.a021816, **PMID:** 26637287, **PMCID:** PMC4743080

Oberauer, K. (2002). Access to information in working memory: Exploring the focus of attention. *Journal of Experimental Psychology: Learning, Memory, and Cognition*, *28*, 411–421. **DOI:** https://doi.org/10.1037/0278-7393.28.3.411, **PMID:** 12018494

Oberauer, K., & Bialkova, S. (2009). Accessing information in working memory: Can the focus of attention grasp two elements at the same time? *Journal of Experimental Psychology: General*, *138*, 64–87. **DOI:** https://doi.org/10.1037/a0014738, **PMID:** 19203170

Palva, S., & Palva, J. M. (2011). Functional roles of alpha-band phase synchronization in local and large-scale cortical networks. *Frontiers in Psychology*, *2*, 204. **DOI:** https://doi.org/10.3389/fpsyg.2011.00204, **PMID:** 21922012, **PMCID:** PMC3166799

Parto Dezfouli, M., Davoudi, S., Knight, R. T., Daliri, M. R., & Johnson, E. L. (2021). Prefrontal lesions disrupt oscillatory signatures of spatiotemporal integration in working memory. *Cortex*, *138*, 113–126. **DOI:** https://doi.org/10.1016/j.cortex.2021.01.016, **PMID:** 33684625

Parto Dezfouli, M., Zarei, M., Constantinidis, C., & Daliri, M. R. (2021). Task-specific modulation of PFC activity for matching-rule governed decision-making. *Brain Structure & Function*, *226*, 443–455. **DOI:** https://doi.org/10.1007/s00429-020-02191-7, **PMID:** 33398431

Perrin, F., Pernier, J., Bertrand, O., & Echallier, J. (1989). Spherical splines for scalp potential and current density mapping. *Electroencephalography and Clinical Neurophysiology*, *72*, 184–187. **DOI:** https://doi.org/10.1016/0013-4694(89)90180-6, **PMID:** 2464490

Poch, C., Capilla, A., Hinojosa, J. A., & Campo, P. (2017). Selection within working memory based on a color retro-cue modulates alpha oscillations. *Neuropsychologia*, *106*, 133–137. **DOI:** https://doi.org/10.1016/j.neuropsychologia.2017.09.027, **PMID:** 28958909

Poncet, F., Baudouin, J.-Y., Dzhelyova, M. P., Rossion, B., & Leleu, A. (2019). Rapid and automatic discrimination between facial expressions in the human brain. *Neuropsychologia*, *129*, 47–55. **DOI:** https://doi.org/10.1016/j.neuropsychologia.2019.03.006, **PMID:** 30885642

Qi, X.-L., Elworthy, A. C., Lambert, B. C., & Constantinidis, C. (2014). Representation of remembered stimuli and task information in the monkey dorsolateral prefrontal and posterior parietal cortex. *Journal of Neurophysiology*, *113*, 44–57. **DOI:** https://doi.org/10.1152/jn.00413.2014, **PMID:** 25298389, **PMCID:** PMC4294574

Roux, F., & Uhlhaas, P. J. (2014). Working memory and neural oscillations: Alpha–gamma versus theta–gamma codes for distinct WM information? *Trends in Cognitive Sciences*, *18*, 16–25. **DOI:** https://doi.org/10.1016/j.tics.2013.10.010, **PMID:** 24268290

Sauseng, P., Klimesch, W., Heise, K. F., Gruber, W. R., Holz, E., Karim, A. A., et al. (2009). Brain oscillatory substrates of visual short-term memory capacity. *Current Biology*, *19*, 1846–1852. **DOI:** https://doi.org/10.1016/j.cub.2009.08.062, **PMID:** 19913428

Schneider, D., Mertes, C., & Wascher, E. (2016). The time course of visuo-spatial working memory updating revealed by a retro-cuing paradigm. *Scientific Reports*, *6*, 21442. **DOI:** https://doi.org/10.1038/srep21442, **PMID:** 26869057, **PMCID:** PMC4751472

Souza, A. S., & Oberauer, K. (2016). In search of the focus of attention in working memory: 13 Years of the retro-cue effect. *Attention, Perception, & Psychophysics*, *78*, 1839–1860. **DOI:** https://doi.org/10.3758/s13414-016-1108-5, **PMID:** 27098647

Sporns, O. (2018). Graph theory methods: applications in brain networks. *Dialogues in Clinical Neuroscience*, *20*, 111–121. **DOI:** https://doi.org/10.31887/DCNS.2018.20.2/osporns, **PMID:** 30250388, **PMCID:** PMC6136126

Sreenivasan, K. K., Curtis, C. E., & D'Esposito, M. (2014). Revisiting the role of persistent neural activity during working memory. *Trends in Cognitive Sciences*, *18*, 82–89. **DOI:** https://doi.org/10.1016/j.tics.2013.12.001, **PMID:** 24439529, **PMCID:** PMC3964018

Stuss, D. T. (2006). Frontal lobes and attention: Processes and networks, fractionation and integration. *Journal of the International Neuropsychological Society*, *12*, 261–271. **DOI:** https://doi.org/10.1017/S1355617706060358, **PMID:** 16573859

Stuss, D. T. (2011). Functions of the frontal lobes: relation to executive functions. *Journal of the International Neuropsychological Society*, *17*, 759–765. **DOI:** https://doi.org/10.1017/S1355617711000695, **PMID:** 21729406

Stuss, D. T., & Knight, R. T. (2013). *Principles of frontal lobe function*. Oxford University Press. **DOI:** https://doi.org/10.1093/med/9780199837755.001.0001

Szczepanski, S. M., & Knight, R. T. (2014). Insights into human behavior from lesions to the prefrontal cortex. *Neuron*, *83*, 1002–1018. **DOI:** https://doi.org/10.1016/j.neuron.2014.08.011, **PMID:** 25175878, **PMCID:** PMC4156912

Vaidya, A. R., Pujara, M. S., Petrides, M., Murray, E. A., & Fellows, L. K. (2019). Lesion studies in contemporary neuroscience. *Trends in Cognitive Sciences*, *23*, 653–671. **DOI:** https://doi.org/10.1016/j.tics.2019.05.009, **PMID:** 31279672, **PMCID:** PMC6712987

Van Diepen, R., Foxe, J. J., & Mazaheri, A. (2019). The functional role of alpha-band activity in attentional processing: The current zeitgeist and future outlook. *Current Opinion in Psychology*, *29*, 229–238. **DOI:** https://doi.org/10.1016/j.copsyc.2019.03.015, **PMID:** 31100655

van Ede, F. (2018). Mnemonic and attentional roles for states of attenuated alpha oscillations in perceptual working memory: A review. *European Journal of Neuroscience*, *48*, 2509–2515. **DOI:** https://doi.org/10.1111/ejn.13759, **PMID:** 29068095, **PMCID:** PMC6220786

van Wijk, B., Jha, A., Penny, W., & Litvak, V. (2015). Parametric estimation of cross-frequency coupling. *Journal of Neuroscience Methods*, *243*, 94–102. **DOI:** https://doi.org/10.1016/j.jneumeth.2015.01.032, **PMID:** 25677405, **PMCID:** PMC4364621

van Wingerden, M., van der Meij, R., Kalenscher, T., Maris, E., & Pennartz, C. M. (2014). Phase-amplitude coupling in rat orbitofrontal cortex discriminates between correct and incorrect decisions during associative learning. *Journal of Neuroscience*, *34*, 493–505. **DOI:** https://doi.org/10.1523/JNEUROSCI.2098-13.2014, **PMID:** 24403149, **PMCID:** PMC6608158

Viswanathan, V., Bharadwaj, H. M., & Shinn-Cunningham, B. G. (2019). Electroencephalographic signatures of the neural representation of speech during selective attention. *eNeuro*, *6*. **DOI:** https://doi.org/10.1523/ENEURO.0057-19.2019, **PMID:** 31585928, **PMCID:** PMC6873161

Wianda, E., & Ross, B. (2019). The roles of alpha oscillation in working memory retention. *Brain and Behavior*, *9*, e01263. **DOI:** https://doi.org/10.1002/brb3.1263, **PMID:** 30887701, **PMCID:** PMC6456781

Zaksas, D., & Pasternak, T. (2006). Directional signals in the prefrontal cortex and in area MT during a working memory for visual motion task. *Journal of Neuroscience*, *26*, 11726–11742. **DOI:** https://doi.org/10.1523/JNEUROSCI.3420-06.2006, **PMID:** 17093094, **PMCID:** PMC6674769